Overexpression of carbonyl reductase 1 in ovarian cancer cells suppresses proliferation and activates the eIF2 signaling pathway

YUKA KADONOSAWA[1], MINAKO YOKOYAMA[1], YOTA TATARA[2], TOSHITSUGU FUJITA[3] and YOSHIHITO YOKOYAMA[1]

[1]Department of Obstetrics and Gynecology, Hirosaki University Graduate School of Medicine, Hirosaki, Aomori 036-8562, Japan; [2]Department of Stress Response Science, Center for Advanced Medical Research, Hirosaki University Graduate School of Medicine, Hirosaki, Aomori 036-8562, Japan; [3]Department of Biochemistry and Genome Biology, Hirosaki University Graduate School of Medicine, Hirosaki, Aomori 036-8562, Japan

Received November 13, 2023; Accepted April 16, 2024

DOI: 10.3892/ol.2024.14492

Abstract. High expression of carbonyl reductase 1 (CBR1) protein in ovarian cancer cells inhibits tumor growth and metastasis. However, the underlying mechanism is unknown. To investigate the mechanism by which CBR1 suppresses tumor growth, the present study generated ovarian cancer cells that constitutively overexpress human CBR1 (hCBR1) protein. Ovarian cancer cell lines (OVCAR-3 and SK-OV-3) were transfected with a plasmid encoding hCBR1, followed by selection with G418 to isolate hCBR1-overexpressing lines. The proliferation rates of hCBR1-overexpressing cells were then compared with those of negative control and wild-type cells. Overexpression of hCBR1 led to significant inhibition of proliferation ($P<0.05$). Subsequently, to investigate changes in intracellular signaling pathways, cellular proteins were extracted and subjected to proteome analysis using liquid chromatography followed by mass spectrometry. There was an inverse correlation between CBR1 protein expression and cell proliferation. In addition, Ingenuity Pathway Analysis of hCBR1-overexpressing cell lines was performed, which revealed changes in the expression of proteins involved in signaling pathways related to growth regulation. Of these, the eukaryotic translation initiation factor 2 (eIF2) signaling pathway was upregulated most prominently. Thus, alterations in multiple tumor-related signaling pathways, including eIF2 signaling, may lead to growth suppression. Taken together, the present data may lead to the development of new drugs that target CBR1 and related signaling pathways, thereby improving outcomes for patients with ovarian cancer.

Correspondence to: Dr Minako Yokoyama, Department of Obstetrics and Gynecology, Hirosaki University Graduate School of Medicine, 5 Zaifu-cho, Hirosaki, Aomori 036-8562, Japan
E-mail: mnk0704@hirosaki-u.ac.jp

Abbreviations: CBR1, carbonyl reductase 1; hCBR1, human CBR1; eIF, eukaryotic translation initiation factor; tGFP, turbo green fluorescent protein; LC-MS/MS, liquid chromatography followed by mass spectrometry; p-eIF2, phosphorylated-eIF2; HRP, horseradish peroxidase; IPA, Ingenuity Pathway Analysis; TC, ternary complex; PKR, protein kinase R; PERK, protein kinase RNA-like endoplasmic reticulum kinase; GCN2, general control nonderepressible-2; HRI, heme-regulated inhibitor; ATF4, activating transcription factor 4; mTOR, mechanistic target of rapamycin; Ab, antibody

Key words: CBR1, ovarian cancer, eIF2, growth regulation, proteome analysis

Introduction

Carbonyl reductase 1 (CBR1), an NADPH-dependent monomeric cytosolic enzyme with wide specificity for carbonyl compounds (1), is expressed in the intestinal tract, liver, kidneys, skin, and ovaries (2,3), where it reduces carbonyl compounds such as anthracyclines, daunorubicin, doxorubicin, and prostaglandins (3). Studies suggest that its primary function is regulation of fatty acid metabolism (3).

CBR1 expression levels are associated with cancer cell malignancy; for example, reduced expression is accompanied by a fall in expression of E-cadherin along with activation of matrix metalloproteinases, which promotes cell proliferation and tumorigenesis of ovarian, cervical, and endometrial cancers *in vivo* (4-6). Previously, we reported that the prognosis for patients with ovarian cancer showing low expression of CBR1 is worse than that of those with ovarian cancer overexpressing CBR1 (4). In addition, increased expression of CBR1 suppresses growth of ovarian cancer cells (6), whereas decreased expression promotes growth and metastasis (5). Our previous study also suggests that increased expression of CBR1 in ovarian cancer cells may exert antitumor effects by activating caspase pathways (6). CBR1 suppresses development of cervical cancer, uterine sarcoma, and non-small cell lung carcinoma (7-9). Taken together, these data suggest that CBR1 regulates fatty acid metabolism and suppresses tumor growth via different molecular mechanisms; however, the signaling cascades affected by changes in CBR1 expression have not been examined in detail.

Proteomics analysis involves systematic, comprehensive, and quantitative identification of the proteins (i.e., the proteome) present in a biological system (e.g., cells, tissues,

organs, fluids, and whole organisms) at a specific point in time (10-12). The three main branches of proteomics used to characterize the function and location of proteins are (I) functional proteomics, (II) structural proteomics, and (III) expression proteomics. The information obtained can be used to predict new proteins involved in signal transduction and disease pathogenesis (13). Therefore, proteomics should be useful for elucidating the molecular mechanisms affected by increased or decreased expression of CBR1.

In this study, we used a proteomics analysis approach to examine signaling cascades altered by stable overexpression of CBR1 in ovarian cancer cells. The workflow of the study is shown in Fig. 1. We generated human ovarian cancer cell lines stably expressing human CBR1 (hCBR1), and then investigated whether their growth was inhibited. We then used liquid chromatography followed by mass spectrometry (LC-MS/MS) to identify the molecules/signaling pathways affected.

Materials and methods

Cell lines and cell culture. OVCAR-3 and SK-OV-3 cell lines were purchased from the American Type Culture Collection (HTB-161 and HTB-77, respectively; Rockville, MD, USA). These cell lines are derived from human ovarian cancer cell tissue and are often used to generate solid tumor xenografts (10,14-18). The cells were cultured in RPMI-1640 medium (Sigma-Aldrich, St Louis, MO, USA) at 37˚C in a water-saturated atmosphere containing 5% CO_2/95% air. The culture medium was supplemented with 10% fetal bovine serum (NICHIREI Biosciences, Tokyo, Japan), 100 U/ml penicillin, and 100 μg/ml streptomycin.

Preparation of plasmid DNA. The pCMV6-AC-GFP-hCBR1 plasmid (RG204950, OriGene Technologies, Inc., Rockville, MD, USA) was used to generate hCBR1-overexpressing cells. This plasmid encodes hCBR1 fused to turbo green fluorescent protein (hCBR1-tGFP), which is expressed under the control of the CMV promoter. Plasmid pCMV6-AC-GFP (PS100010, OriGene Technologies, Inc.), which expresses tGFP, was used to generate negative control cell lines.

Transfection of ovarian cancer cells. Ovarian cancer cells were plated into a 10 cm dish and cultured to 70-80% confluence. Cells were then transfected with 24 μg of pCMV6-AC-GFP-hCBR1 or pCMV6-AC-GFP using Lipofectamine 3000 (Life Technologies, Rockville, MD, USA) for 24 h at 37˚C. Then, G418 (NACALAI TESQUE, Inc., Kyoto, Japan) was added (0.4 mg/ml) to the culture medium to select cell lines possessing the plasmid DNA in their genome.

Immunoblot analysis. Cells were homogenized on ice in radio-immunoprecipitation assay (RIPA) buffer (Fujifilm Wako, Osaka, Japan) containing cOmplete Mini EDTA-free Protease Inhibitor Cocktail Tablets provided in EASY packs (Roche, Basel, Switzerland). Protein measurements were performed using Bio-Rad Protein Assay Dye Reagent Concentrate (Bio-Rad Laboratories, Hercules, CA, USA). Proteins (8 μg) were loaded into the wells of 5-20% SDS-polyacrylamide gels (Fujifilm Wako), electrophoresed, and transferred to polyvinylidene difluoride membranes. The membranes were blocked for 1 h at room temperature with Tris-buffered saline (TBS) containing 0.05% Tween-20/1% skim milk or 2% bovine serum albumin [for the anti-phospho-translation initiation factor 2 (eIF2)α blot] and then incubated overnight at 4˚C with a polyclonal rabbit anti-hCBR1 antibody (Ab) (1:1,000; ab-186825; Abcam, Cambridge, UK), an anti-β-actin Ab (1:5,000; M177-3; MBL, Tokyo, Japan), an anti-eIF2α Ab (1:5,000; 9722, Cell Signaling Technology, Danvers, MA, USA), an anti-phospho-eIF2α (p-eIF2α) Ab (1:5,000; 9721, Cell Signaling Technology), and an anti-activating transcription factor 4 (ATF4) Ab (1:1,000; ab-216839; Abcam). After washing with TBS/0.05% Tween-20, the membranes were incubated for 1 h at room temperature with an appropriate horseradish peroxidase (HRP)-conjugated secondary Ab [either anti-mouse IgG-HRP (NA9310V; GE Healthcare, Pittsburgh, PA, USA) or anti-rabbit IgG-HRP (NA9340V; GE Healthcare)]. Protein bands were detected using enhanced chemiluminescence (Image Quant LAS4000 system; GE Healthcare). The detected bands were quantified using Image J (19).

Evaluation of ovarian cancer cell proliferation. Wild-type, negative control, and hCBR1-tGFP-overexpressing ovarian cancer cells were plated in 6 cm dishes ($1.0x10^4$ cells/dish) and cultured at 37˚C for 24, 48, 72, 96, or 120 h. Cells were then washed with 1 ml of Dulbecco's phosphate-buffered saline and detached with 0.5 g/l-Trypsin/0.53 mmol/l-EDTA Solution (NACALAI TESQUE, Inc., Kyoto, Japan). Trypan blue solution (0.1%; NACALAI TESQUE, Inc.) was used to discriminate living from dead cells; cells were counted using a hemocytometer (Bio Medical Science, Tokyo, Japan). The rate of cell growth was calculated as the slope of a linear fit created by plotting the natural logarithm of the cell number against culture time.

LC-MS/MS. Wild-type OVCAR-3 and five lots of OVCAR-3-derived cells overexpressing CBR1 were cultured and sampled in triplicate. Cell lysates were prepared as described for immunoblot analysis. Label-free whole cell proteomic analysis was performed as described previously (20). Briefly, cell lysates containing 20 μg of total protein, as determined by the bicinchoninic acid (BCA) method, were denatured with acetone. The precipitates were then denatured with 50% trifluoroethanol. Disulfide bonds were reduced with dithiothreitol (DTT) and alkylated with iodoacetamide followed by trypsin digestion. After desalting and purification of the resulting peptides using MonoSpin C18 columns (GL Sciences Inc., Tokyo, Japan), the samples were subjected to LC-MS/MS using a nanoLC system (Eksigent 400, AB Sciex, Framingham, MA, USA) coupled online to a mass spectrometer (TripleTOF6600, AB Sciex). Peptide separation was performed using LC on a nano C18 reverse-phase capillary tip column (75 μm x 125 mm, 3 μm, Nikkyo Technos CO., Tokyo, Japan) at 300 nl/min with a 90 min linear gradient of 8-30% acetonitrile in 0.1% FA, and then, with a 10 min linear gradient of 30 to 40% acetonitrile in 0.1% FA. The mass spectrometer was operated in information-dependent acquisition (IDA) and data-independent acquisition (SWATH) while in positive ion mode, scanning full spectra (400-1,500 m/z) for

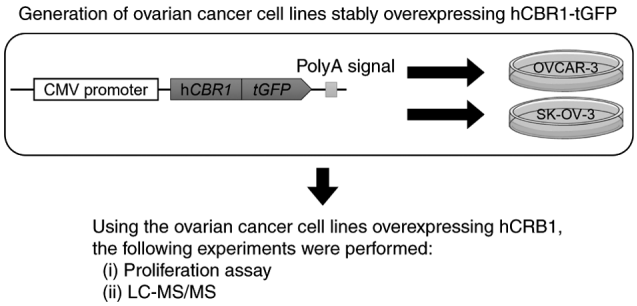

Figure 1. Study workflow. Ovarian cancer cell lines (OVCAR-3 and SK-OV-3) stably overexpressing hCBR1 fused to turbo green fluorescent protein (hCBR1-tGFP) were established and then used for subsequent experiments. CBR1, carbonyl reductase 1; hCBR1, human CBR1; tGFP, turbo green fluorescent protein; LC-MS/MS, liquid chromatography followed by mass spectrometry.

250 msec, followed by up to 30 MS/MS scans (100-1,800 m/z for 50 msec each), for a cycle time of 1.8 sec. Candidate ions with a charge state between +2 and +5 and counts above a minimum threshold of 125 counts per second were isolated for fragmentation, and one MS/MS spectrum was collected before adding those ions to the exclusion list for 12 sec. For SWATH acquisition, the parameters were set as follows: 100 msec TOF MS scan, followed by 200 variable SWATH windows each at 50 msec accumulation time for m/z 400-1,250. MS/MS SWATH scans were set at 5 Da window overlapping by 1 Da for m/z 400-1,250 and varied on each side of the mass range. The total cycle time was 9.6 sec. A rolling collision energy parameters script was used to automatically control the collision energy. Database searching for acquired spectra was performed using ProteinPilot 5.0.1 software (AB Sciex). The positive identification threshold was set at a false discovery rate of 1% or less. The resulting library file and SWATH (data independent acquisition) files were processed by PeakView (ver. 2.2.0, AB Sciex) and exported to MarkerView (ver. 1.3.0.1; AB Sciex). The peak area of individual proteins was normalized relative to the sum of the peak areas of all detected proteins.

Statistical analysis and reproducibility. Experiments were performed in triplicate for immunoblot analysis and evaluation of ovarian cancer cell proliferation. Normal distribution was tested by Shapiro-Wilk test. Statistical differences between the three groups (hCBR1-tGFP-overexpressing, negative control, and wild-type cells) were analyzed using one-way ANOVA followed by Tukey's test (parametric data) or Kruskal-Wallis test (non-parametric data). $P<0.05$ was considered to indicate a statistically significant difference. All statistical analyses were performed using IBM SPSS ver. 29.0 statistics software (IBM, Chicago, Illinois).

Regarding the statistical analysis of the proteome data, principal component analysis using SIMCA software (version 15.0.2, Infocom Corp., Tokyo, Japan) confirmed that there was no outlier proteome in any of the samples. Since the cell lines used show endogenous CBR1 expression, proteins covarying with CBR1 were subjected to Spearman's rank correlation analysis and Pearson's correlation analysis (R version 4.1.0 software) to capture proteomic variations due to CBR1 transfection. Proteins with FDR-adjusted $P<0.05$ were identified as proteins covarying with CBR1 and subjected to pathway enrichment and network analysis by Ingenuity Pathway Analysis (IPA) software (Qiagen, Venlo, Netherland).

Results

Generation of ovarian cancer cells stably expressing hCBR1-tGFP. To investigate the role of CBR1 on the malignancy of ovarian cancer cells, we first generated OVCAR-3 and SK-OV-3 cell lines stably expressing hCBR1-tGFP. We also generated ovarian cancer cells expressing only tGFP as a control (negative control cells). Immunoblot analysis using an anti-CBR1 Ab revealed stable expression of hCBR1-tGFP (Figs. 2A and 3A). A band corresponding to hCBR1-tGFP was not observed in the negative control and wild-type cell samples. We measured CBR1 protein expression levels (i.e., the combined expression levels of hCBR1-tGFP and CBR1) in OVCAR-3 and SK-OV-3 cells using image analysis software (Figs. 2B and 3B). The results confirmed that expression of CBR1 protein in hCBR1-tGFP-overexpressing OVCAR-3 cells was significantly higher than that in wild-type and negative control cells (Fig. 2B). As to SK-OV-3 cells, hCBR1-tGFP-overexpressing cell #1 and #2 showed the highest and relatively high expression of CBR1 protein, respectively (Fig. 3B). Although all hCBR1-tGFP-overexpressing SK-OV-3 cells showed hCBR1-tGFP expression (Fig. 3A), the expression was slight in the cell line #4. Therefore, statistical significance on the total CBR1 amount was not observed among cell groups (Fig. 3B). Nevertheless, hCBR1-tGFP was visibly expressed in the cell line #4, and the other hCBR1-tGFP-expressing cells show a tendency of upregulation of total hCBR1 protein. To examine the importance of the CBR1 protein in ovarian cancer cells, these established SK-OV-3 cells were also used for subsequent experiments.

Antiproliferative effects of CBR1. To evaluate the effect of CBR1 overexpression on tumor cell growth, we measured proliferation of OVCAR-3 and SK-OV-3 cells expressing hCBR1-tGFP. As shown in Fig. 4A and B, growth of OVCAR-3 and SK-OV-3 cells expressing hCBR1-tGFP was slower than that of wild-type or negative control cells. These results suggest that overexpression of hCBR1 strongly inhibits growth of ovarian cancer cells, although it should be noted that overexpression of tGFP alone moderately affected growth of SK-OV-3 cells (Fig. 4B). hCBR1-tGFP-overexpressing OVCAR-3 cells showed significant suppression of cell proliferation ($P<0.05$, vs. negative control or wild-type) (Fig. 4A). hCBR1-tGFP-overexpressing SK-OV-3 cells also showed significant suppression of cell proliferation ($P<0.05$, vs. negative control or wild-type, Fig. 4B). As to SK-OV-3 cells, differences in cellular growth were also observed between wild-type and negative control cells ($P<0.05$, Fig. 4B). Because tGFP is potentially cytotoxic (21), expression of tGFP may also affect the growth of SK-OV-3 cells.

In hCBR1-tGFP-overexpressing OVCAR-3, we confirmed an inverse correlation between hCBR1 overexpression and cell proliferation (Fig. 4C). In the hCBR1-tGFP-overexpressing lines

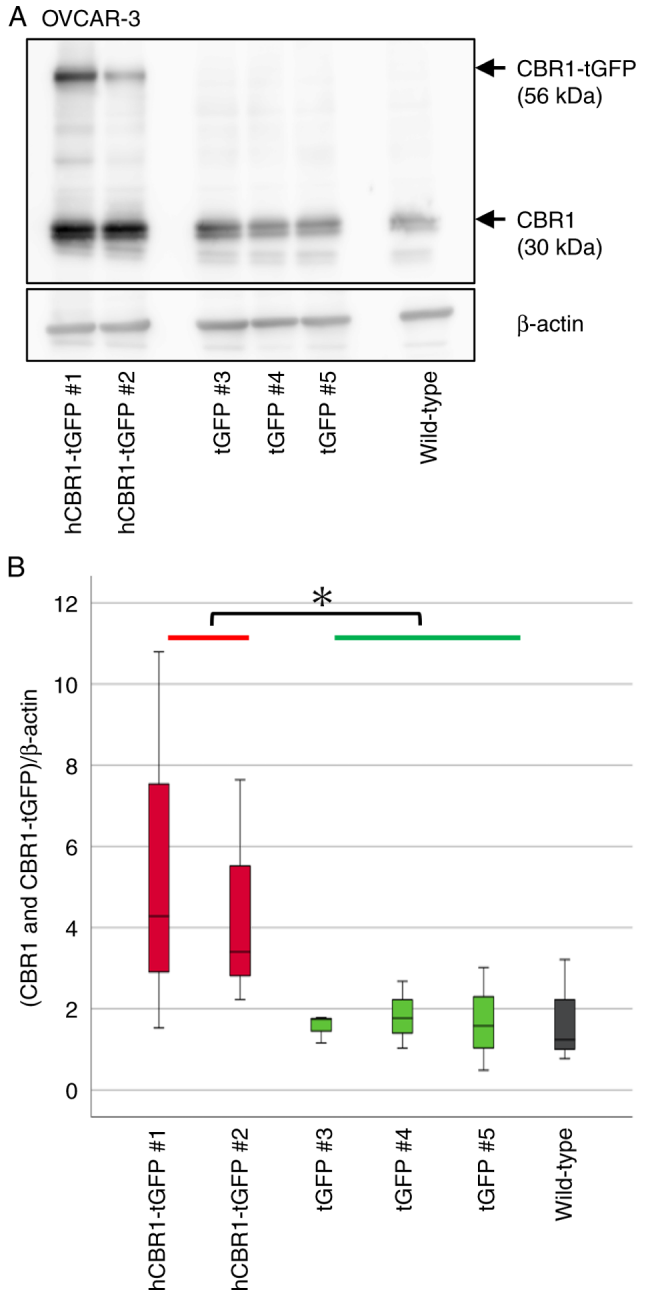

Figure 2. Establishment of OVCAR-3 cell lines stably overexpressing hCBR1-tGFP. (A and B) Expression of CBR1 protein in the established OVCAR-3 cells. (A) Expression of CBR1 was evaluated by immunoblot analysis. Anti-CBR1 antibody was used to detect hCBR1-tGFP and endogenous CBR1. β-actin was detected as an internal control. Two hCBR1-tGFP-overexpressing OVCAR-3 lines and three negative control cell lines were analyzed. (B) Expression of CBR1 protein in A (CBR1 and CBR1-tGFP) was quantified using Image J. Data are normalized to expression of β-actin. *P<0.05. CBR1, carbonyl reductase 1; hCBR1, human CBR1; tGFP, turbo green fluorescent protein.

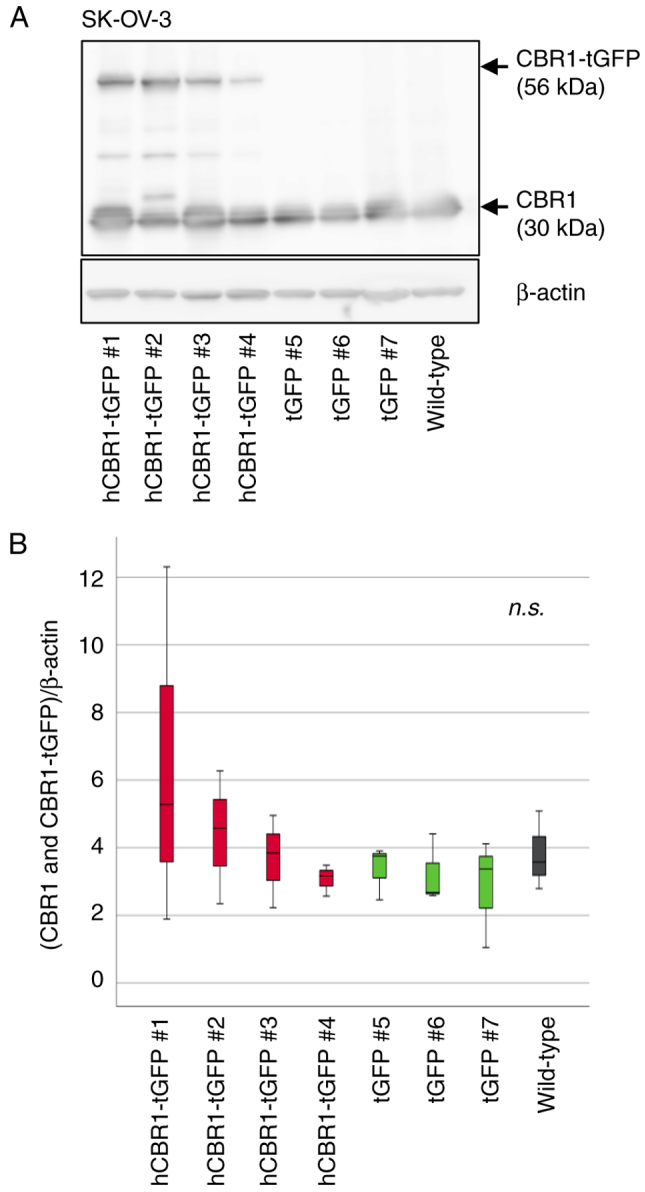

Figure 3. Establishment of SK-OV-3 cell lines stably overexpressing hCBR1-tGFP. (A and B) Expression of CBR1 protein in the established SK-OV-3 cells. (A) Expression of CBR1 was evaluated by immunoblot analysis. Anti-CBR1 antibody was used to detect hCBR1-tGFP and endogenous CBR1. β-actin was detected as an internal control. Four hCBR1-tGFP-overexpressing SK-OV-3 lines and three negative control cell lines were analyzed. (B) Expression of CBR1 protein in A (CBR1 and CBR1-tGFP) was quantified using Image J. Data are normalized to expression of β-actin. n.s., not significant. CBR1, carbonyl reductase 1; hCBR1, human CBR1; tGFP, turbo green fluorescent protein.

(#1, #2), CBR1 expression levels were high, and the cell proliferation rate was reduced. By contrast, negative control cells (#3-#5) and wild-type cells expressed low levels of CBR1 and showed higher proliferation rates. In these experiments, CBR1 expression is the sum of endogenous CBR1 and exogenous hCBR1-tGFP, and the higher levels of CBR1 protein in hCBR1-tGFP-overexpressing lines are consistent with the results shown in Fig. 1B. Thus, these results support the above data showing that hCBR1-tGFP-overexpressing lines grow more slowly than negative control and wild-type cells (Fig. 4A). Previously, we showed that transient expression of CBR1 in a xenograft mouse model may induce apoptosis through activation of caspase pathways (6). Thus, stable overexpression of hCBR1-tGFP may induce apoptosis in OVCAR-3 and SK-OV-3 cells.

Altered intracellular signaling in hCBR1-tGFP-overexpressing cancer cell lines. To elucidate the CBR1-mediated molecular mechanism underlying growth inhibition, we performed LC-MS/MS of OVCAR-3 cell lysates, followed by IPA. Whole cell proteomics analysis using a label-free quantification method plus MS resulted in quantification of 939 proteins, with

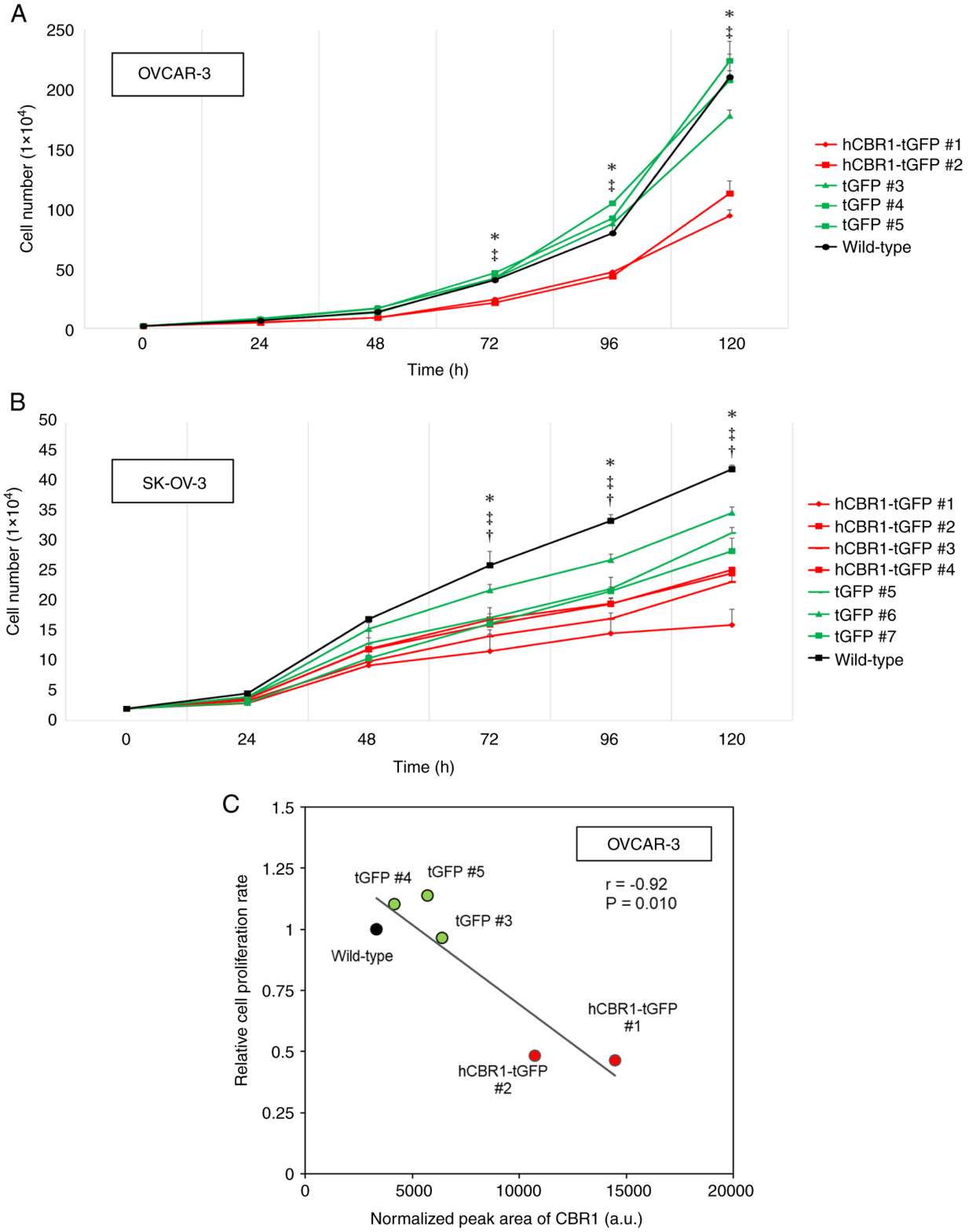

Figure 4. Inhibitory effects of CBR1 on growth of ovarian cancer cells. (A and B) Proliferation of hCBR1-tGFP-overexpressing (A) OVCAR-3 and (B) SK-OV-3 cells. Cell numbers were counted at each time point. *P<0.05, hCBR1-tGFP (#1 and #2) vs. tGFP (#3-#5) for OVCAR-3, or hCBR1-tGFP (#1-#4) vs. tGFP (#5-#7) for SK-OV-3, ‡P<0.05, hCBR1-tGFP (#1 and #2) vs. Wild-type for OVCAR-3, or hCBR1-tGFP (#1-#4) vs. Wild-type for SK-OV-3, †P<0.05, tGFP (#5-#7) vs. Wild-type. (C) Correlation between the normalized peak area of CBR1 measured in proteome analysis and cell proliferation rate relative to wild-type. The X and Y axes depict arbitrary values. The semi-quantitative amount of CBR1 is shown as the sum of endogenous CBR1 expression and exogenous hCBR1-tGFP expression. Cell proliferation rate was represented as the number of cells increased per hour relative to wild-type. a.u., arbitrary unit. CBR1, carbonyl reductase 1; hCBR1, human CBR1; tGFP, turbo green fluorescent protein.

no samples showing outliers upon principal component analysis (Fig. S1). Of these, the abundance of 155 proteins correlated significantly with expression of hCBR1 (FDR-adjusted P-value <0.05, Spearman's rank correlation, Fig. S2). We then performed

Table I. Top 20 signaling pathways affected by overexpression of CBR1 in OVCAR-3 cells.

Ingenuity canonical pathway	-log (P-value)	Ratio
eIF2 signaling	20.3	0.103
mTOR signaling	6.77	0.052
Regulation of eIF4 and p70S6K signaling	6.50	0.056
Coronavirus pathogenesis pathway	5.08	0.044
Mitochondrial dysfunction	4.74	0.047
CSDE1 signaling pathway	4.47	0.089
Spliceosomal cycle	3.52	0.082
Pentose phosphate pathway (Oxidative Branch)	3.37	0.400
FAT10 signaling pathway	3.29	0.071
Gluconeogenesis I	3.19	0.115
Leukocyte extravasation signaling	2.75	0.031
tRNA charging	2.67	0.077
Pentose phosphate pathway	2.64	0.182
BAG2 signaling pathway	2.64	0.048
Sirtuin signaling pathway	2.49	0.024
VEGF signaling	2.38	0.040
Inhibition of ARE-mediated mRNA degradation pathway	2.37	0.031
Virus entry via endocytic pathways	2.30	0.039
Germ cell-sertoli cell junction signaling	2.26	0.029
Oxidative phosphorylation	2.20	0.036

The 155 proteins whose expression correlated with hCBR1 expression were analyzed by Ingenuity Pathway Analysis. The top 20 out of 65 canonical pathways that were enriched significantly are shown. The ratio of the number of proteins correlated with hCBR1 to the number of proteins registered in the canonical pathway is shown as the 'Ratio'. The higher this value, the more relevant the pathway. hCBR1, human carbonyl reductase 1.

IPA to identify enriched canonical pathways associated with hCBR1-correlated proteins; the top 20 pathways are shown in Table I. Expression of proteins involved in various signaling pathways, whose role in controlling tumor progression is suggested, correlated with expression of hCBR1. Among these, the eIF2 signaling pathway was the most enriched.

The z-score for the eIF2 signaling pathway, as calculated by IPA, was +1.387. The z-score indicates whether the detected signal is biased toward activation or inactivation, with positive values indicating activation and negative values indicating inactivation (Fig. S3). Table I shows that eIF2 signaling is highly affected by overexpression of hCBR1. Proteins associated with eIF2 signaling are listed in Table II. Of the 23 proteins associated with eIF2 signaling, 17 had positive correlation coefficients.

We also used IPA to perform a protein-protein interaction network analysis of hCBR1-correlated proteins. The top 35 out of the 155 proteins whose expression correlated with that of CBR1 were extracted in the order of interaction network robustness and presented as a subnetwork (Fig. 5). Among the 35 proteins, 15 formed a subnetwork related to eIF2 signaling, as shown by the cyan borders. These results suggest that the eIF2 signaling pathway may be involved in suppressing cell growth.

eIF2 phosphorylation status in OVCAR-3 cells stably expressing hCBR1-tGFP. Next, we investigated whether the eIF2 signaling pathway is actually altered by overexpression of hCBR1-tGFP. Considering the magnitude of changes in eIF2 signaling, and the critical importance of phosphorylation status of eIF2 during regulation of the pathway (Fig. 6A, see also the Discussion section) (22), we performed immunoblot analysis to examine phosphorylation of eIF2α, a subunit of eIF2. A clear band corresponding to p-eIF2α was observed in lysates prepared from hCBR1-tGFP-expressing cells (#1, #2) (Fig. 6B-a), confirming that overexpression of hCBR1 induces phosphorylation of eIF2α. Expression and phosphorylation of eIF2α protein in OVCAR-3 cells were quantified using image analysis software. The results confirmed that the phosphorylation levels of eIF2α in hCBR1-tGFP-overexpressing cells were higher than those in wild-type and negative control cells (Fig. 6B-b).

Phosphorylation of eIF2α downregulates general translation and upregulates expression of ATF4 (Fig. 6A) (22). Although we examined involvement of ATF4 downstream of eIF2α, we found that expression of ATF4 was not upregulated in hCBR1-tGFP-expressing cells (Fig. 6C). Therefore, overexpression of hCBR1 may induce downregulation of general translation via phosphorylation of eIF2α.

Discussion

In this study, we generated ovarian cancer cells stably expressing hCBR1-tGFP. Proliferation of hCBR1-tGFP-overexpressing cells was slower than that of negative control and wild-type

Table II. Proteins associated with eIF2 signaling.

Gene symbol	UniProt ID	Protein name	Correlation coefficient	-$\log_{10}$ (P-value)
EIF1AX	Q8BMJ3	Eukaryotic translation initiation factor 1A	0.344	1.8
EIF3F	Q9DCH4	Eukaryotic translation initiation factor 3 subunit F	0.414	2.5
PTBP1	P17225	Polypyrimidine tract-binding protein 1	-0.349	1.8
RPL10	Q6ZWV3	60S ribosomal protein L10	0.399	2.3
RPL11	Q9CXW4	60S ribosomal protein L11	0.404	2.4
RPL13	P47963	60S ribosomal protein L13	0.328	1.6
RPL14	Q9CR57	60S ribosomal protein L14	-0.291	1.3
RPL18A	P62717	60S ribosomal protein L18a	0.340	1.7
RPL23	P62830	60S ribosomal protein L23	0.392	2.2
RPL23A	P62751	60S ribosomal protein L23a	0.286	1.3
RPL24	Q8BP67	60S ribosomal protein L24	0.418	2.5
RPL27A	P14115	60S ribosomal protein L27a	0.337	1.7
RPL31	P62900	60S ribosomal protein L31	-0.315	1.5
RPL34	Q9D1R9	60S ribosomal protein L34	0.497	3.5
RPL7A	P12970	60S ribosomal protein L7a	-0.465	3.1
RPS10	P63325	40S ribosomal protein S10	0.320	1.6
RPS12	P63323	40S ribosomal protein S12	0.422	2.6
RPS15	P62843	40S ribosomal protein S15	0.324	1.6
RPS15A	P62245	40S ribosomal protein S15a	0.285	1.3
RPS25	P62852	40S ribosomal protein S25	0.333	1.7
RPS29	P62274	40S ribosomal protein S29	0.392	2.2
RPS9	Q6ZWN5	40S ribosomal protein S9	-0.341	1.8
RRAS2	P62071	Ras-related protein R-Ras2	-0.299	1.4

Twenty-three proteins are associated with eIF2 signaling. Most of the correlation coefficients are positive.

cells. To elucidate the mechanism of cell growth suppression by CBR1 overexpression, we used proteomics together with IPA. The results showed marked differences in the expression of proteins involved in eIF2 signaling in hCBR1-tGFP-overexpressing cells. Concordantly, constitutive phosphorylation of eIF2α, which plays a critical role in eIF2 signaling, suggests that CBR1 regulates cell growth via the eIF2 signaling pathway.

Generally, it is accepted that protein synthesis drives the cell cycle (23). The relationship between regulation of protein synthesis and cancer cell growth has attracted considerable attention because regulation of mRNA translation is a convergence point for many oncogenic signals (24). The eIF2 signaling pathway plays a central role in regulating general translation in response to stress. eIF2 comprises three subunits: α, β, and γ. GTP-bound eIF2 interacts with the initiating methionyl-tRNA (ternary complex, TC) and transports it to the 40S ribosome (25). The elF2 translation initiation complex integrates a variety of stress-related signals to downregulate general translation, but it upregulates translation of specific mRNAs such as that encoding *ATF4* (26). In this regard, because we did not show upregulation of ATF4 protein, it may be that overexpression of CBR1 downregulates general translation.

Phosphorylation of eIF2α is induced by a diverse family of four stress-activated kinases: protein kinase R (PKR) [induced by dsRNA], protein kinase RNA-like endoplasmic reticulum kinase (PERK) [induced by endoplasmic reticulum (ER) stress], general control nonderepressible-2 (GCN2) [induced by amino acid starvation], and heme-regulated inhibitor (HRI) [induced by heme deficiency] (Fig. 6A). As a limitation of this study, we could not confirm how CBR1 induces phosphorylation of eIF2α. Therefore, it would be interesting to examine this issue in future. We examined only one downstream eIF2α pathway-related molecule (ATF4) in this study. Therefore, we would like to examine the other downstream molecules and related physiological changes, including oxidative stress-induced reactive oxygen species generation, in a future study. On the other hand, in addition to OVCAR-3, hCBR1-tGFP-overexpressing SK-OV-3 cells were established in this study. Although all hCBR1-tGFP-overexpressing cells showed hCBR1-tGFP expression, statistical significance was not achieved as a group, which may also be a limitation of this study.

Initiation of protein synthesis is regulated by two rate-limiting steps: assembly of eukaryotic translation initiation factor 4F (eIF4F) and formation of the TC. Assembly of eIF4F is promoted by mechanistic target of rapamycin (mTOR) signaling (27). It is interesting to note that IPA revealed that within the proteome of hCBR1-tGFP-overexpressing cells, factors involved in mTOR signaling were among those whose levels changed (Table I), although it is unclear whether mTOR signaling fluctuates upwards or downwards (Fig. S3). Since the eIF2 signaling pathway and mTOR signaling are

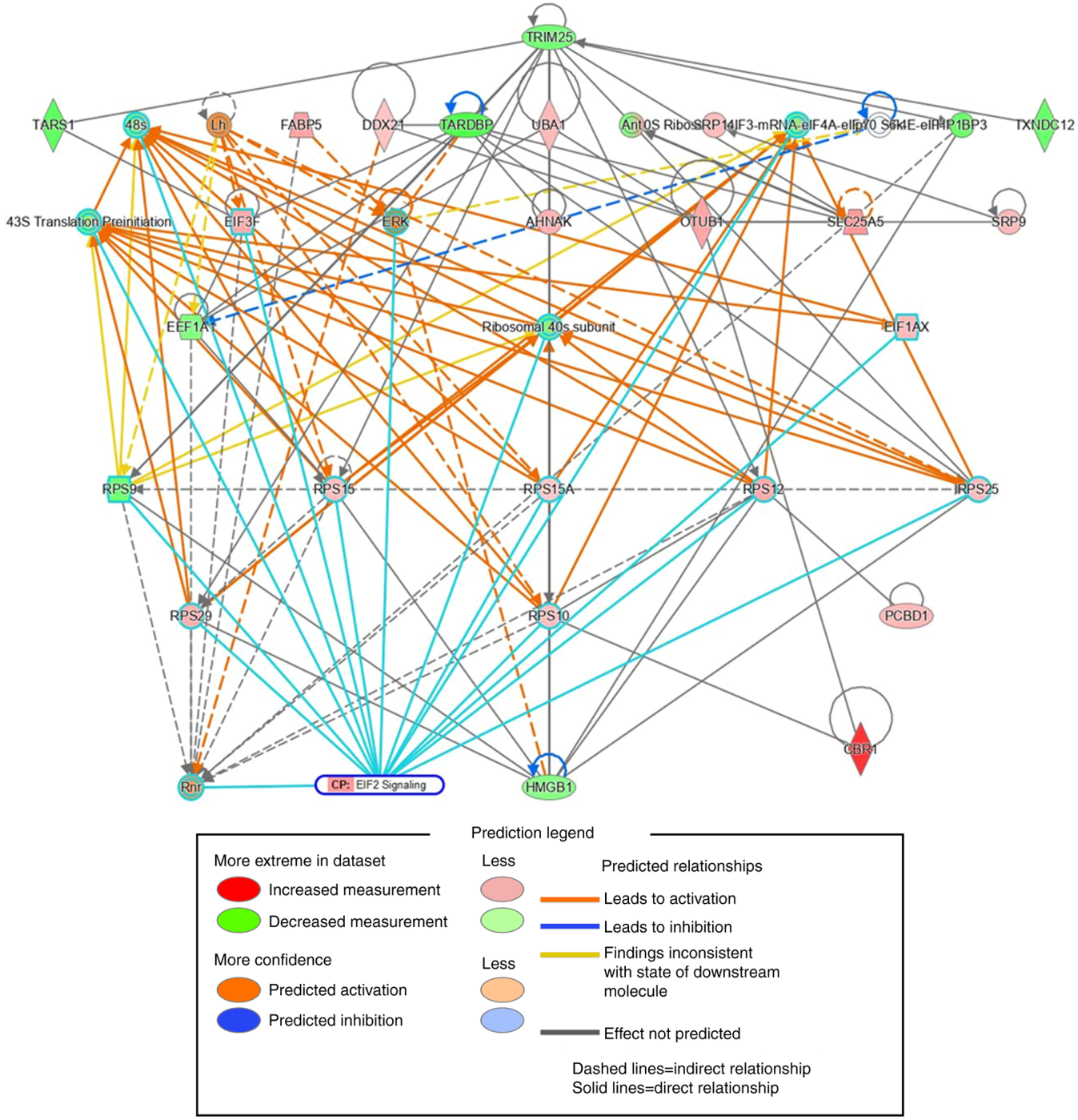

Figure 5. Regulatory associations between protein-protein networks, based on the IPA Knowledge Base. The top 35 of the 155 proteins whose expression correlated with that of CBR1 were extracted in the order of interaction network robustness and presented as a subnetwork. The red and green nodes indicate a positive or negative correlation with CBR1 expression, respectively. The node shapes denote enzymes (diamond), transporters (trapezoid), and other (cycle) proteins. Solid and dashed lines represent direct and indirect interactions, respectively. Nodes involved in eIF2 signaling are highlighted by cyan borders. CP: Canonical pathways.

exquisitely coordinated to provide a robust response to cellular stress (28-30), overexpression of CBR1 may affect both pathways to suppress growth of ovarian cancer cells.

In this study, we demonstrated regulation of the eIF2 signaling pathway by CBR1. Although further studies are needed, our data suggest a new therapeutic strategy for ovarian cancer based on targeting CBR1 and related signaling cascades. This could be achieved by developing molecularly targeted drugs directed at components of the eIF2 signaling pathway, as well as CBR1 itself. In addition, CBR1 may be a potential biomarker of medical prognosis.

Acknowledgements

The authors would like to thank Dr Hodaka Fujii (Hirosaki University Graduate School of Medicine), for helpful discussion and critical reading of the manuscript. They also would

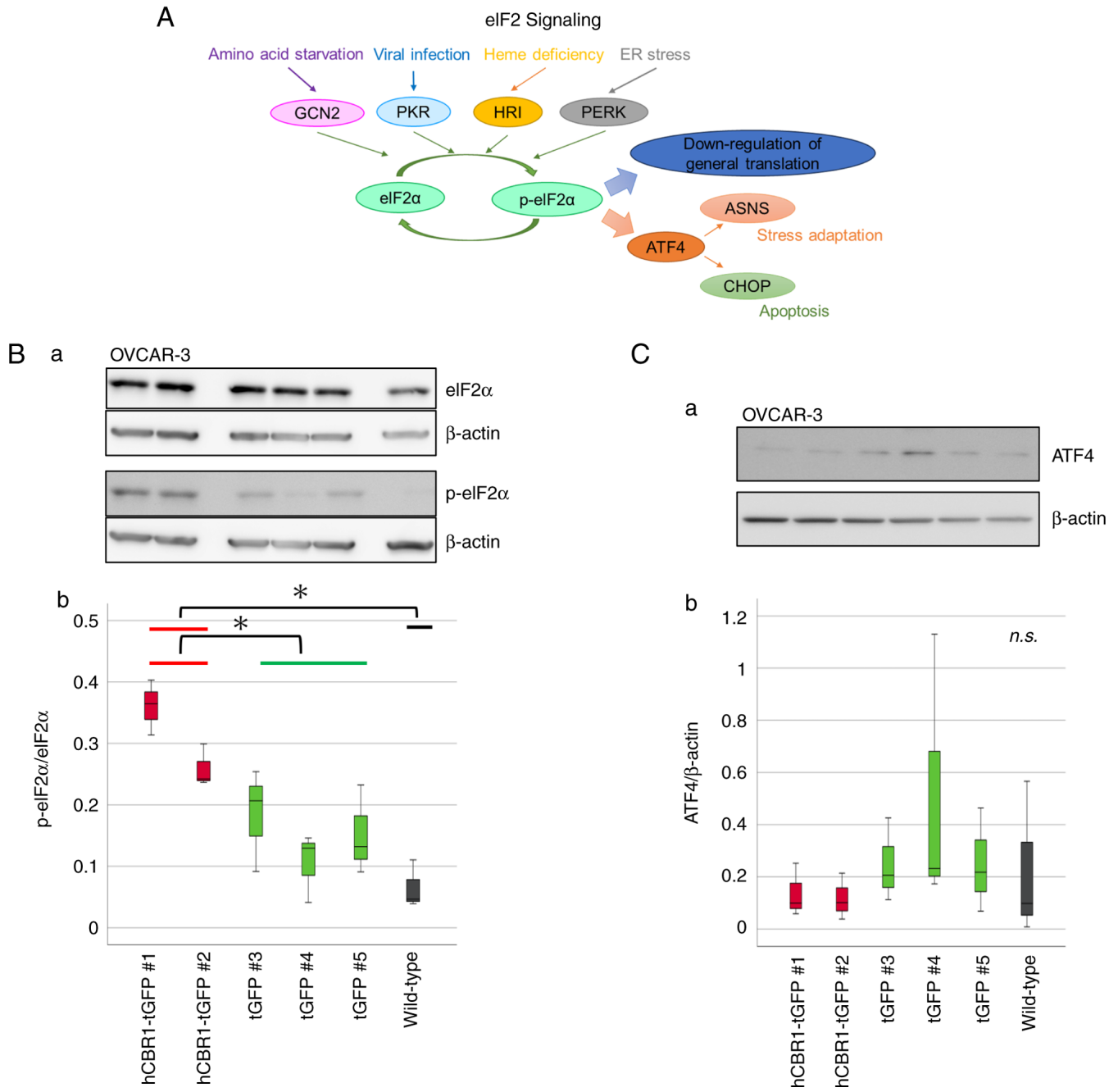

Figure 6. The eIF2 signaling pathway and phosphorylation of eIF2α in hCBR1-tGFP-overexpressing OVCAR-3 cells. (A) Schematic diagram of the eIF2 signaling pathway. Four kinases of eIF2α have been identified in humans: GCN2, PKR, HRI, and PERK. Phosphorylation of eIF2α leads to apoptosis and autophagy via ASNS or CHOP. (B-a) Immunoblot analysis to detect phosphorylation of the eIF2α protein. (B-b) The detected bands were quantified using ImageJ. The ratio of the band intensity (i.e., p-eIF2α: eIF2α) is shown. *P<0.05. (C-a) Immunoblot analysis of ATF-4 protein expression. (C-b) The ratio of the band intensity (i.e., ATF-4: β-actin) is shown. n.s., not significant. Each antibody reaction was performed on each membrane. eIF2, eukaryotic translation initiation factor 2; hCBR1, human carbonyl reductase 1; tGFP, turbo green fluorescent protein; GCN2, general control nonderepressible-2; PKR, protein kinase R; HRI, heme-regulated inhibitor; PERK, protein kinase RNA-like endoplasmic reticulum kinase; ASNS, aspartate synthetase; CHOP, C/EBP homologous protein; p-eIF2, phosphorylated-eIF2; ATF-4, activating transcription factor 4.

like to thank Ms. Miyu Miyazaki (Center for Scientific Equipment Management, Hirosaki University Graduate School of Medicine), for technical support with mass spectrometry.

Funding

This work was supported by a JSPS KAKENHI grant (grant no. 20K09589, to YY).

Availability of data and materials

The proteomics data generated in the present study may be found in the Proteome Xchange and jPOST Repositor databases under accession numbers PXD039299 and JPST001979, respectively or at the following URLs: https://proteomecentral.proteomexchange.org/cgi/GetDataset?ID=PXD039299 and https://repository.jpostdb.org/entry/JPST001979.2. The other data generated in the present study may be requested from the corresponding author.

Authors' contributions

YK, MY and YY conceived the project. TF and YY designed and supervised the project. YT performed LC-MS/MS analysis. YK and MY performed the other experiments. YK, MY, TF and YY wrote the manuscript. YK and MY confirm the authenticity of all the raw data. All authors read and approved the final version of the manuscript.

Ethics approval and consent to participate

Not applicable.

Patient consent for publication

Not applicable.

Competing interests

The authors declare that they have no competing interests.

References

1. Mindnich RD and Penning TM: Aldo-keto reductase (AKR) superfamily: Genomics and annotation. Hum Genomics 3: 362-370, 2009.
2. Fagerberg L, Hallström BM, Oksvold P, Kampf C, Djureinovic D, Odeberg J, Habuka M, Tahmasebpoor S, Danielsson A, Edlund K, *et al*: Analysis of the human tissue-specific expression by genome-wide integration of transcriptomics and antibody-based proteomics. Mol Cell Proteomics 13: 397-406, 2014.
3. Wermuth B, Bohren KM, Heinemann G, von Wartburg JP and Gabbay KH: Human carbonyl reductase. Nucleotide sequence analysis of a cDNA and amino acid sequence of the encoded protein. J Biol Chem 263: 16185-16188, 1988.
4. Umemoto M, Yokoyama Y, Sato S, Tsuchida S, Al-Mulla F and Saito Y: Carbonyl reductase as a significant predictor of survival and lymph node metastasis in epithelial ovarian cancer. Br J Cancer 85: 1032-1036, 2001.
5. Osawa Y, Yokoyama Y, Shigeto T, Futagami M and Mizunuma H: Decreased expression of carbonyl reductase 1 promotes ovarian cancer growth and proliferation. Int J Oncol 46: 1252-1258, 2015.
6. Miura R, Yokoyama Y, Shigeto T, Futagami M and Mizunuma H: Inhibitory effect of carbonyl reductase 1 on ovarian cancer growth via tumor necrosis factor receptor signaling. Int J Oncol 47: 2173-2180, 2015.
7. Nishimoto Y, Murakami A, Sato S, Kajimura T, Nakashima K, Yakabe K, Sueoka K and Sugino N: Decreased carbonyl reductase 1 expression promotes tumor growth via epithelial mesenchymal transition in uterine cervical squamous cell carcinomas. Reprod Med Biol 17: 173-181, 2018.
8. Kajimura T, Sato S, Murakami A, Hayashi-Okada M, Nakashima K, Sueoka K and Sugino N: Overexpression of carbonyl reductase 1 inhibits malignant behaviors and epithelial mesenchymal transition by suppressing TGF-β signaling in uterine leiomyosarcoma cells. Oncol Lett 18: 1503-1512, 2019.
9. Takenaka K, Ogawa E, Oyanagi H, Wada H and Tanaka F: Carbonyl reductase expression and its clinical significance in non-small-cell lung cancer. Cancer Epidemiol Biomarkers Prev 14: 1972-1975, 2005.
10. Graves PR and Haystead TA: Molecular biologist's guide to proteomics. Microbiol Mol Biol Rev 66: 39-63, 2002.
11. Chandramouli K and Qian PY: Proteomics: Challenges, techniques and possibilities to overcome biological sample complexity. Hum Genomics Proteomics 8: 239204, 2009.
12. Wang D, Eraslan B, Wieland T, Hallström B, Hopf T, Zolg DP, Zecha J, Asplund A, Li LH, Meng C, *et al*: A deep proteome and transcriptome abundance atlas of 29 healthy human tissues. Mol Syst Biol 15: e8503, 2019.
13. Martínez-Rodríguez F, Limones-González JE, Mendoza-Almanza B, Esparza-Ibarra EL, Gallegos-Flores PI, Ayala-Luján JL, Godina-González S, Salinas E and Mendoza-Almanza G: Understanding cervical cancer through proteomics. Cells 10: 1854, 2021.
14. Shigeto T, Yokoyama Y, Xin B and Mizunuma H: Peroxisome proliferator-activated receptor α and γ ligands inhibit the growth of human ovarian cancer. Oncol Rep 18: 833-840, 2007.
15. Wakui M, Yokoyama Y, Wang H, Shigeto T, Futagami M and Mizunuma H: Efficacy of a methyl ester of 5-aminolevulinic acid in photodynamic therapy for ovarian cancers. J Cancer Res Clin Oncol 136: 1143-1150, 2010.
16. Cebulla J, Huuse EM, Pettersen K, van der Veen A, Kim E, Andersen S, Prestvik WS, Bofin AM, Pathak AP, Bjørkøy G, *et al*: MRI reveals the in vivo cellular and vascular response to BEZ235 in ovarian cancer xenografts with different PI3-kinase pathway activity. Br J Cancer 112: 504-513, 2015.
17. Zalewski M, Kulbacka J, Saczko J, Drag-Zalesinska M and Choromanska A: Valspodar-modulated chemotherapy in human ovarian cancer cells SK-OV-3 and MDAH-2774. Bosn J Basic Med Sci 19: 234-241, 2019.
18. Lu T, Tang J, Shrestha B, Heath BR, Hong L, Lei YL, Ljungman M and Neamati N: Up-regulation of hypoxia-inducible factor antisense as a novel approach to treat ovarian cancer. Theranostics 10: 6959-6976, 2020.
19. Ohgane K and Yoshioka H: Quantification of gel bands by an image J Macro, Band/Peak Quantification Tool v1. Protocols.io: 2019 doi: /10.17504/protocols.io.7vghn3w.
20. Yokoyama M, Fujita T, Kadonosawa Y, Tatara Y, Motooka D, Ikawa M, Fujii H and Yokoayama Y: Development of transgenic mice overexpressing mouse carbonyl reductase 1. Mol Biol Rep 50: 531-540, 2023.
21. Costantini LM, Fossati M, Francolini M and Snapp EL: Assessing the tendency of fluorescent proteins to oligomerize under physiologic conditions. Traffic 13: 643-649, 2013.
22. Boye E and Grallert B: eIF2α phosphorylation and the regulation of translation. Curr Genet 66: 293-297, 2020.
23. Johnston GC, Pringle JR and Hartwell LH: Coordination of growth with cell division in the yeast Saccharomyces cerevisiae. Exp Cell Res 105: 79-98, 1977.
24. Kovalski JR, Kuzuoglu-Ozturk D and Ruggero D: Protein synthesis control in cancer: selectivity and therapeutic targeting. EMBO J 41: e109823, 2022.
25. Clemens MJ and Bommer UA: Translational control: The cancer connection. Int J Biochem Cell Biol 31: 1-23, 1999.
26. Hinnebusch AG: Molecular mechanism of scanning and start codon selection in eukaryotes. Microbiol Mol Biol Rev 75: 434-467, 2011.
27. Harris AL: Hypoxia-a key regulatory factor in tumour growth. Nat Rev Cancer 2: 38-47, 2002.
28. Hinnebusch AG: The scanning mechanism of eukaryotic translation initiation. Annu Rev Biochem 83: 779-812, 2014.
29. Gandin V, Masvidal L, Cargnello M, Gyenis L, McLaughlan S, Cai Y, Tenkerian C, Morita M, Balanathan P, Jean-Jean O, *et al*: mTORC1 and CK2 coordinate ternary and eIF4F complex assembly. Nat Commun 7: 11127, 2016.
30. Wengrod J, Wang D, Weiss S, Zhong H, Osman I and Gardner LB: Phosphorylation of eIF2α triggered by mTORC1 inhibition and PP6C activation is required for autophagy and is aberrant in PP6C-mutated melanoma. Sci Signal 8: ra27, 2015.